CORROSION SCIENCE AND TECHNOLOGY, Vol.16, No.4(2017), pp.194~200 pISSN: 1598-6462 / eISSN: 2288-6524
[Research Paper] DOI: https://doi.org/10.14773/cst.2017.16.4.194

Detection of SCC by Electrochemical Noise and In-Situ 3-D Microscopy

Da-Hai Xia[1], Yashar Behnamian[1], Jing-Li Luo[1,†], and Stan Klimas[2]

[1]*Department of Chemical and Materials Engineering, University of Alberta, Edmonton, Alberta, Canada, T6G 1H9*
[2]*Atomic Energy of Canada Ltd, Chalk River Laboratories, Stn. 80, Chalk River, Ontario, Canada, K0J 1J0*

(Received June 14, 2017; Revised June 14, 2017; Accepted July 26, 2017)

Stress-corrosion cracking (SCC) of alloy 600 and alloy 800 in 0.5 mol/L thiosulfate solution during constant strain was investigated using electrochemical noise (EN) combined with 3-D microscope techniques. The in-situ morphology observation and EN results indicate that the SCC process could be divided into three stages: (1) passive film stabilization and growth, (2) crack initiation, (3) and crack growth. Power Spectral Density (PSD) and the probability distribution obtained from EN were used as the "fingerprint" to distinguish the different processes. During passive film stabilization and growth, the current noise signals resembled "white noise": when the crack initiated, many transient peaks could be seen in the current noise and the wavelet energy at low frequency as well as the noise resistance decreased. After crack propagation, the noise amplitudes increased, particularly the white noises at low and high frequencies (W_L and W_H) in the PSDs. Finally, the detection of metal structure corrosion in a simulated sea splash zone and pipeline corrosion in the atmosphere are established.

Keywords: *electrochemical noise, alloy 600, sensor, stress-corrosion cracking*

1. Introduction

Significant corrosion degradation of steam generator (SG) tubing has been found in the SG secondary side worldwide. Pitting corrosion and crevice/underdeposit corrosion, intergranular attack (IGA) and stress corrosion cracking (SCC) are among the possible major forms of degradation for SG tube materials. In the case of outer diameter (OD) SCC of SG tubing, it is found to be mostly associated with packed heat-transfer crevices at tube supports where the dilute impurities can hide out, concentrate and, in some cases, precipitate. Typically, the deposits are mostly porous magnetite, but may also contain copper, lead, sulfur, aluminum, silicon and other species. The crevices can result in a corrosive fluid in the deposit pores. Sulfur is often present, initially as sulfate that can be reduced by hydrazine or by Fe, Cr and Ni to produce aggressive lower valence species [1].

Detection of SCC at early stage is increasingly more important to generate the knowledge to ensure the nuclear power plant operability. It is also very desirable in the context of degradation afflicting numerous other engineered systems. In laboratory settings, investigators have used in-situ physical methods (such as acoustic emission (AE) [2-4]), surface analysis methods (such as Transmission Electron Microscopy (TEM), scanning electron microscope (SEM)), electrochemical methods (such as electrochemical noise (EN) [5,6], electrochemical impedance spectroscopy (EIS) [7]) and a combination of EIS and EN [8-10] to detect SCC. However, the information provided by TEM and SEM may be limited because they are not in-situ methods. EN records the fluctuations in the potential and current generated spontaneously by corrosion processes. In recent years, it has received considerable attention in the corrosion monitoring. EN, associated with all degrees of freedom of the system, indicates a change in the thermodynamic and kinetic states of the interface, and it is the only electrochemical technique that does not disturb the system [11]. It can be used to monitor remotely the corrosion type and intensity. With the progress in electronics and mathematical methods (such as wavelet theory), EN applications that can be used for monitoring and detection of corrosion process have been developed in recent years. The corrosion and corrosion-related processes identified as sources of the EN signal include, among others, the initiation and propagation of stress corrosion cracks [5,8]; hydrogen bubble nucleation, growth, and detachment [12]; passive film formation and growth [13,14]; nucleation, growth, and propagation of pits [15]; abrasion-corrosion [16]; high temperature corro-

† Corresponding author: jingli.luo@ualberta.ca

sion [14,17]; and microbial corrosion [18]; degradation of organic coatings [19,20] and uniform corrosion [21]. Analysis of the spontaneous fluctuations of potential and current is performed to distinguish between the different corrosion processes, because each type of corrosion (for example, general corrosion, pitting, crevice, and stress corrosion cracking) can exhibit a characteristic "fingerprint" or "signature" in the noise signal. This "fingerprint" can be used to identify the type of corrosion occurring and to quantify its severity [22]. Traditional electrochemical techniques such as the linear polarization resistance, electrochemical impedance, etc., cannot provide this kind of information. Therefore, most of the EN development has been directed on localized corrosion. The advantage of EN is that it can monitor ongoing corrosion, for example, "transient peaks" would appear on both potential noise and current noise; the challenging aspect is how to extract interpretable parameters from the EN data. EN is an in-situ electrochemical method based predominantly on statistics, however, modern mathematics such as wavelet analysis [23-25], chaos theory [11,21], Hilbert spectra [26] have also been introduced into the EN analysis in recent years. Online detection in-situ in nuclear power plants at early stages of degradation is of great research interest and an important development tendency. Quirk [27], Kain [28], Hickling [29], and Macak [17,30] successfully detected corrosion and SCC of Alloy 600, 304 stainless steel (SS) and 08CH18N10T austenitic SS in high temperature and high pressure water, and they used noise resistance, spectral noise resistance and frequency analysis to characterize the corrosion behaviour in different solutions and immersion time, and finally they monitored the crack initiation and propagation through the transient features.

In this work, the initiation and propagation of SCC on Alloy 600 and Alloy 800 detected by EN and microscopy, and characteristic parameters are extracted from the EN data using modern algorithms to distinguish different corrosion modes. This in-lab investigation is a step towards a field application of EN.

2. Experimental Procedure

The Alloy 600 tubing used in this investigation (Sandvik, Heat #: 769536) contained Fe (8.98 wt%), Ni

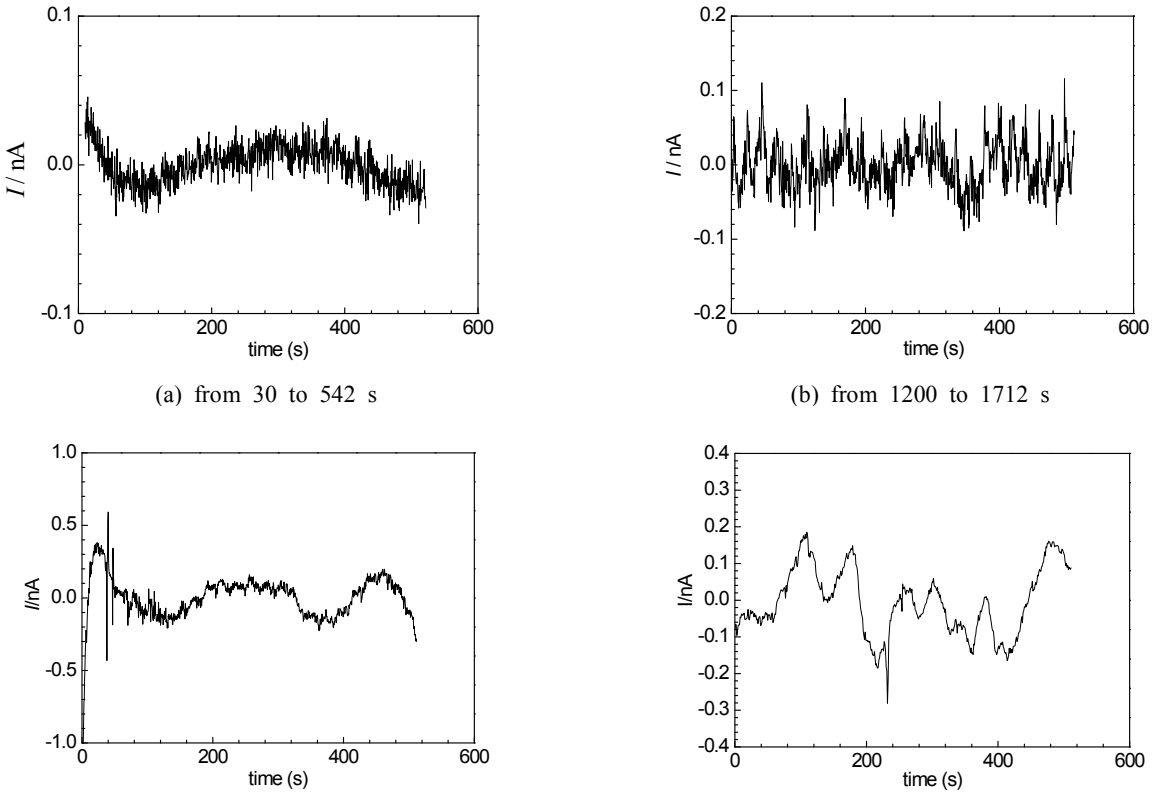

(a) from 30 to 542 s

(b) from 1200 to 1712 s

(c) from 4000 to 4512 s

(d) from 6000 to 6512s

Fig. 1 ECN during the SCC process.

(73.44 wt%), Cr (16.62 wt%) and other low-content elements (Si, Mn, P, S, Co, Ti). It had the dimension of 13.9 mm outer diameter and 1.13 mm average wall thickness. The Alloy 800 tubing (Sandvik Heat #: 516809) contained Fe (43.2 wt%), Ni (32.78 wt%), Cr (21.87 wt%) and other low-content elements (Si, Mn, P, S, Co, Ti) and had the dimension of 15.88 mm outer diameter and 1.13 mm average wall thickness. The Alloy 600 sample was a C-ring of constant strain (deflection on OD: 1.356 mm). In accordance with GB38-01, the applied stress was significantly higher than the Alloy 600 yield stress. Specimens were 20 mm long, connected with copper wire and sealed in epoxy. The end surface of the ring was mechanically polished with wet silicon carbide paper (Buehler Ltd.) down to 1200 grit to expose the end surface of C-ring, then rinsed with copious deionized water, and dried in air. For Alloy 800, a compact tension (CT) sample with a pre-formed crack of 2.578 mm was used.

The EN measurements were conducted using a three-electrode configuration. A saturated calomel electrode (SCE) was used as the reference electrode and a platinum electrode was used as the counter electrode. Before the measurement, the working electrode surface was cathodically polarized at -1 V_{SCE} for 15 min to remove the native oxide and then exposed to an open-circuit for 30 min. Each electrochemical noise test was carried out with a sampling frequency of 2 Hz. Before statistical analysis, the direct current (dc) component was removed from the original EN data by a 5-order polynomial fitting [11] on every 512 s interval.

3. Results and Discussion

3.1 Detection of SCC on Alloy 600 C-ring using EN

Fig. 1 shows the electrochemical current noise (ECN) during the test. The ECN reveals different features as the experiment progresses. In the beginning (see Fig. 1a), the ECN resembles "white noise", and the amplitude of ECN is about 0.02 nA; as the immersion time increases to 1200 s, the amplitude of ECN increases to 0.1 nA. After the immersion time further reaches 4000 s (Fig. 1 c), some transient peaks appear in the ECN data, which are usually an indicator of localized corrosion such as surface passive film breakdown; for the time of 6000 s, more transient peaks are apparent in the EN data.

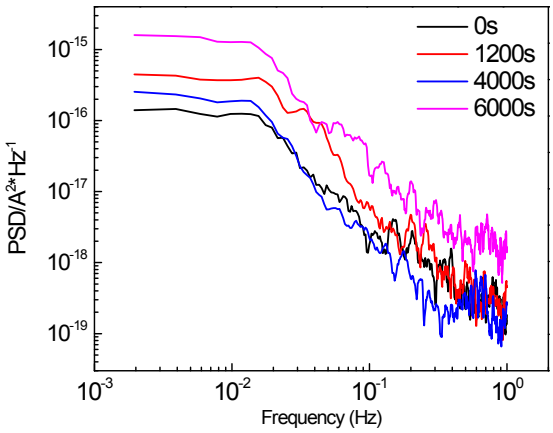

Fig. 2 PSD of ECN during the SCC.

To study the characteristics of EN parameters at different stages of the corrosion process, the EN data from typical time segments during SCC were extracted and analyzed (512 s were chosen for each segment). PSDs obtained by fast Fourier transformation (FFT) are shown in Fig. 2. Table 1 lists the parameters from the PSDs. Uruchurtu [31] has found that, while the roll-off slope of the PSD is much lower than −20 dB dec^{-1}, the material is in uniform corrosion or in passivation state. When the roll-off slope is higher than −20 dB dec^{-1}, it is usually the symptom of localized corrosion. From the value of the roll-off slope, *K*, of the PSD of ECN during the different time segments shown in Fig. 2 and Table 1, before

Table 1 Parameters from PSDs

Number	Time /s	$W_L/10^{-16}V^2 \cdot Hz^{-1}$	$K/dB \cdot dec^{-1}$	$S_I/A \cdot cm^{-2}$
A	30~542	-1.81	-29.25	1.12E-6
B	600~1112	-2.95	-30.36	1.41E-6
C	1200~1712	-3.95	-31.11	1.05E-6
D	2000~2512	-4.37	-23.59	2.13E-6
E	4000~4512	-2.44	-15.85	3.87E-6
F	5000~5512	-10.58	-17.50	3.61E-6
G	6000~6512	-11.44	-18.28	3.21E-6

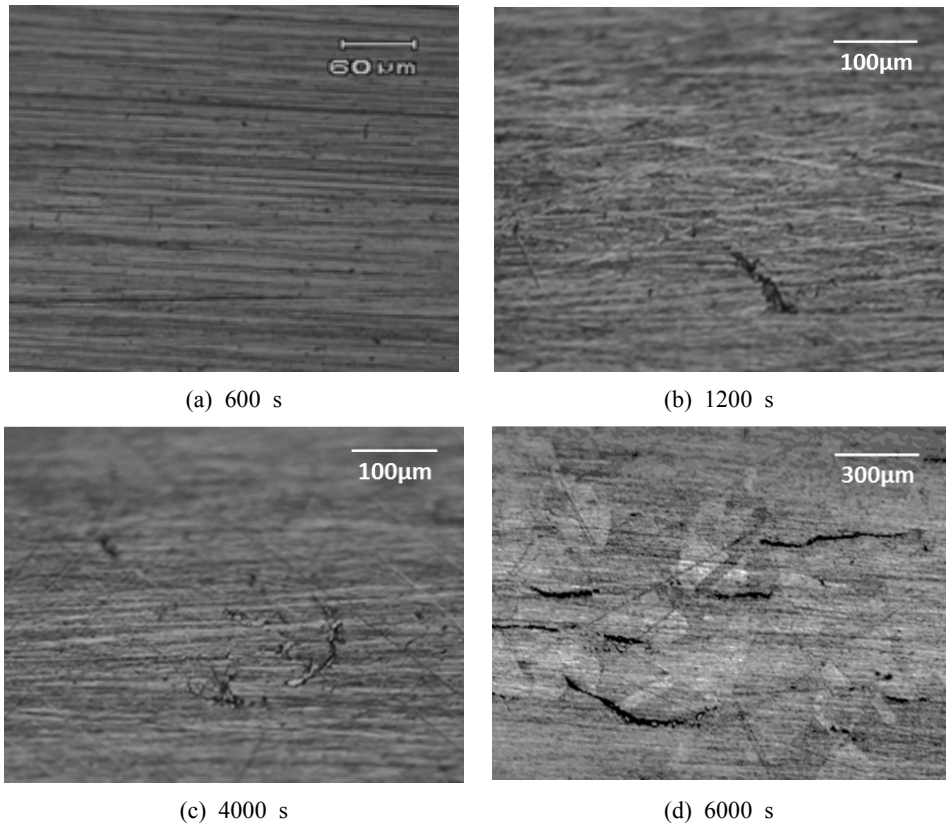

(a) 600 s (b) 1200 s

(c) 4000 s (d) 6000 s

Fig. 3 Surface morphology of Alloy 600 during SCC as a function of time at (a) 600 s, (b) 1200 s, (c) 4000 s, and (d) 6000 s.

4000 s (A, B, C, D time segment), the values of roll-off slope K were all lower than −20 dB dec^{-1}, while the amplitude of ECN were much lower (Fig. 2), which indicates that the surface is in passive state. After 4000 s (E, F, G time segment), as the experiment went on, the values of roll-off slope K were all higher than −20 dB dec^{-1}, while the amplitude of ECN increases markedly (Fig. 1), which indicated that localized corrosion, e.g., pitting and crack propagation, might have occurred on the surface of the specimen. It should be noted that *K* decreases again; the possible reason being that the corrosion products accumulated on the surface of the specimen alleviate the corrosion effect. Surface morphology of the specimen at various stages during the experiment are shown in Fig. 3. It can be observed that no pitting corrosion or cracking appeared in the specimen surface before 600 s (Fig. 3a), consistent with no localized corrosion on the surface of specimen at the initial stage of the experiment. As was seen from Fig. 3c and d, some cracks were observed on the surface of specimen at the later stage of the experiment. Hence, the result of EN data analysis was confirmed by the microscopic observation.

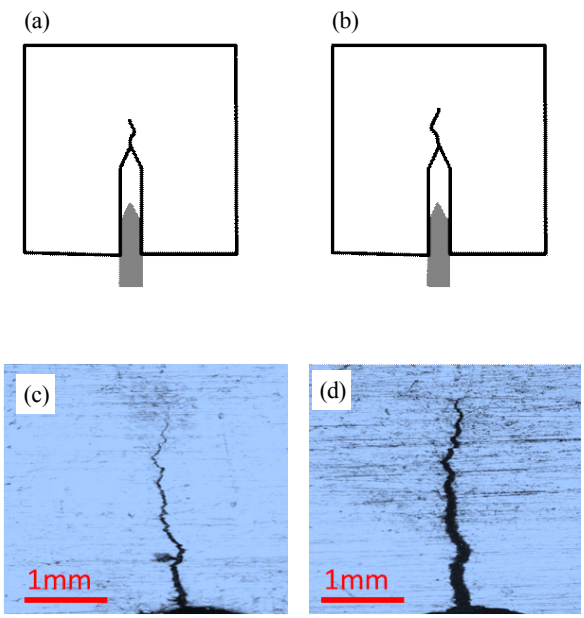

Fig. 4 the CT sample before and after the experiment.

3.2 Detection of SCC on Alloy 800 using EN

Fig. 4a and c shows the Alloy 800 CT sample with a crack of 2.578 mm, and the sample was polarized at

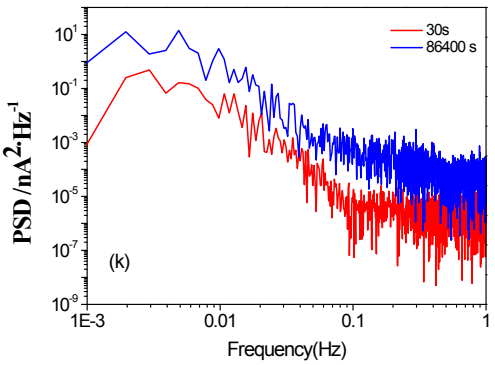

Fig. 5 PSD of ECN during the SCC.

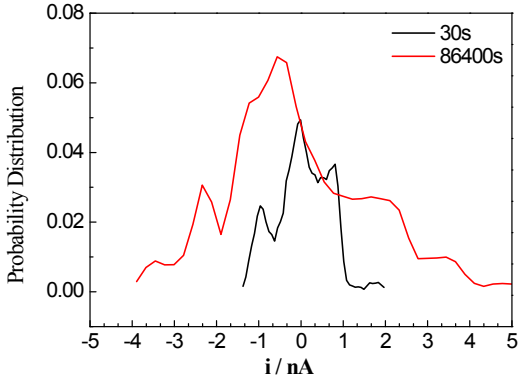

Fig. 6 Probability distribution of ECN.

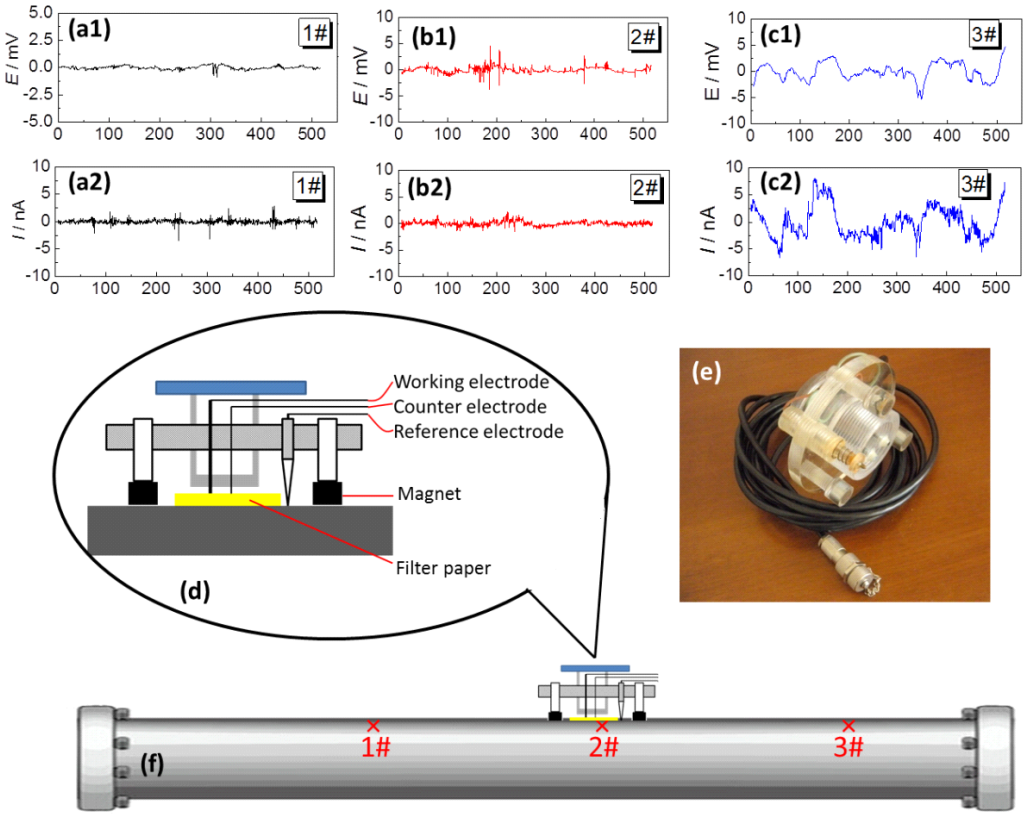

Fig. 7 Detection of the atmospheric corrosion of three sites on pipeline using a EN sensor (a1,a2) EPN and ECN of site 1; (b1,b2) EPN and ECN of site 2; (c1,c2) EPN and ECN of site 3; (d) schematic diagram of the EN sensor; (e) a picture of the sensor; (f) schematic diagram when detecting three different sites using the sensor.

0.9 V_{SCE} for 90000 s. It is observed that, after the experiment, the crack propagated by 0.275 mm. The ECN data sets were recorded at 30 s and 86400 s, respectively. The PSD and probability distribution ECN are shown in Fig. 5 and Fig. 6, respectively. In the process of crack propagation, the noise amplitudes, the white noises at low and high frequencies (W_L and W_H) in the PSDs increase, and the probability distribution of ECN also become wider after the crack propagation.

3.3 Detection of pipeline steel corrosion using EN sensor

Fig. 7 shows data from an electrochemical sensor for monitoring of atmospheric corrosion of pipeline steel. Fig. 7e is a photograph of the sensor. There are three electrodes

in this sensor: PtNb wire as the counter electrode, pure Zn as the reference electrode, and a Cu wire connected to the materials being investigated as the working electrode. The sensor attach to the metal surface by magnets. During the measurement, a filter paper wetted with distilled water was inserted between the sensor and the tested surface, as shown in Fig. 2d. The measured EN data for three different sites are shown in Fig. 7 a-c. It is apparent that site #3 suffers localized corrosion because there are many transient peaks in the EN spectrum taken at that site.

3.4 Detection of corrosion in marine splash zone using electrochemical noise [32]

A splash zone corrosion was simulated in lab and the results are briefly described in this section. Fig. 8 shows a schematic diagram of a test device to simulate the corrosion in marine splash zone. This device was composed of metal frame immersed in a water tank, with a spray nozzle, and the electrochemical sensor. It can simulate the conditions of the full immersion zone, tidal range zone and splash zone. The splash zone simulation could be achieved with a spray nozzle and an outfall at the bottom of the tank. The simu-

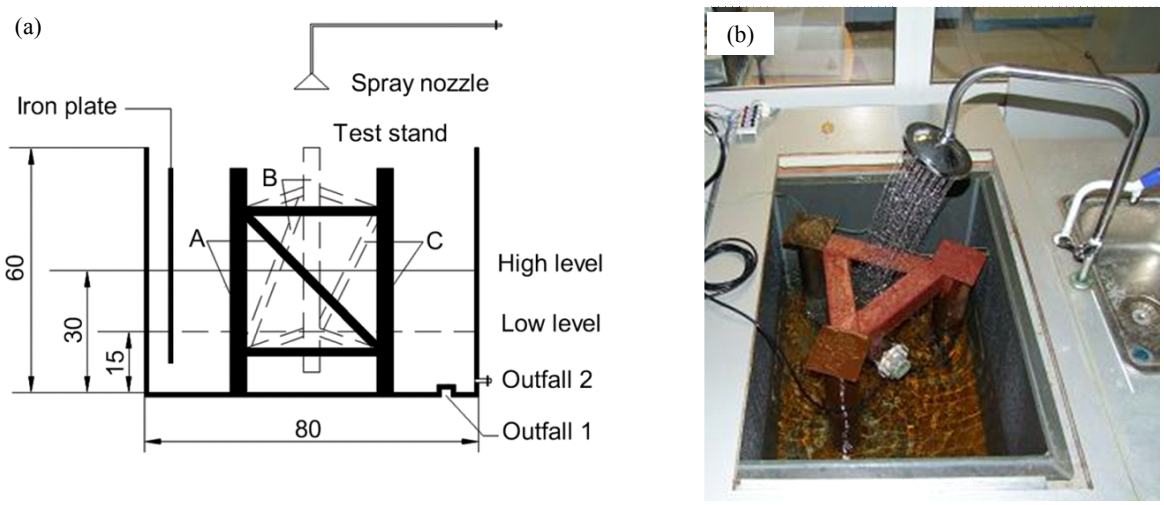

Fig. 8 Schematic diagram of the simulated corrosion test device (unit, cm).

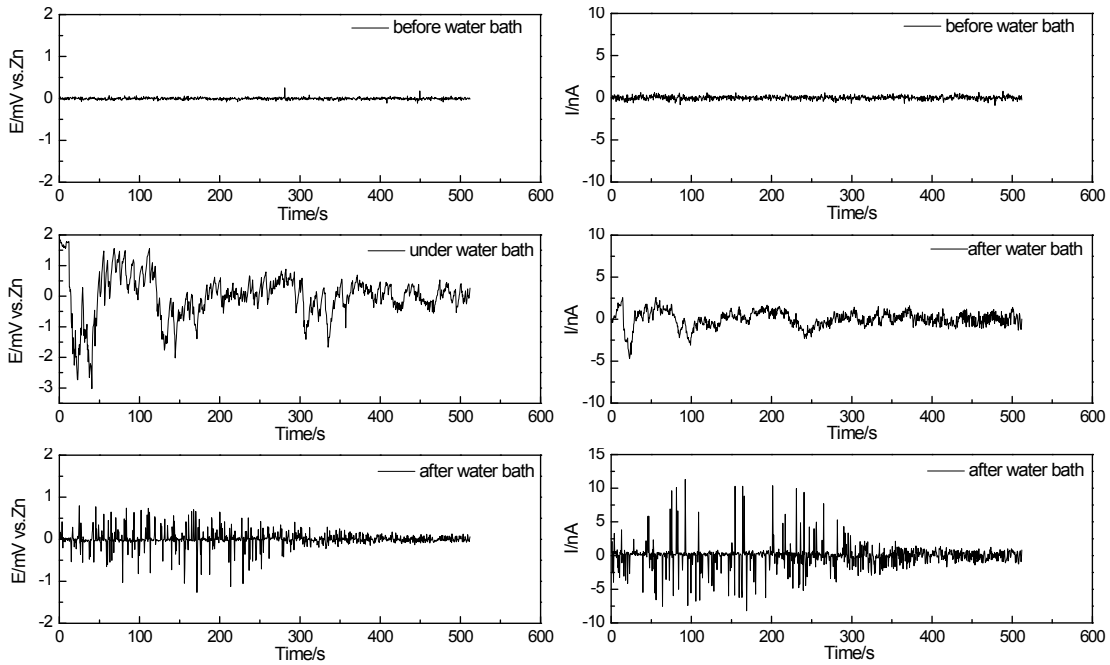

Fig. 9 Time domain spectrum after the trend removal.

lated splash zone corrosion was achieved by controlling the liquid at certain level with opening the spay nozzle and also turning on the outfall at the bottom of the tank at the same time. The metal frame was treated by three methods: part A was the bare metal, part B was coated with a lacquer, and part C was covered by an organic coating which was resistant to marine corrosion. Fig. 9 shows the ECN and EPN before water bath, during water bath and after water bath. It is clear that the amplitude of both EPN and ECN during the water bath and after the water bath are higher than those before the water bath, indicating that the corrosion rate of the investigated metal under these two cases are higher than before the water bath.

4. Conclusions

During passive film stabilization and growth, the current noise signals resembled "white noise"; when the crack initiated, many transient peaks could be seen in current noise, and the wavelet energy at low frequency and noise resistance also decreased. After crack propagation, the noise amplitudes, the white noises at low and high frequencies (W_L and W_H) in the PSDs increased. Laboratory simulation also indicate that the EN technique could be used in the detection of metal structure corrosion in sea splash zone atmospheric corrosion of pipelines.

Acknowledgments

This work was supported Atomic Energy of Canada Ltd (AECL).

References

1. R. W. Staehle and J. A. Gorman, *Corrosion*, **59**, 931 (2003).
2. M. G. Alvarez, P. Lapitz, and J. Ruzzante, *Corros. Sci.*, **55**, 5(2012).
3. A. Etiemble, H. Idrissi, and L. Roue, *Int. J. Hydrogen Energ.*, **38**, 1136 (2013).
4. L. Calabrese, G. Campanella, and E. Proverbio, *Corros. Sci.*, **73**, 161 (2013).
5. M. Breimesser, S. Ritter, H. P. Seifert, T. Suter, and S. Virtanen, *Corros. Sci.*, **63**, 129 (2012).
6. R. Zhao, Z. Zhang, J. B. Shi, L. Tao, and S. Z. Song, *J. Cent. South Univ. T.*, **17**, 13 (2010).
7. A. A. Oskuie, T. Shahrabi, A. Shahriari, and E. Saebnoori, *Corros. Sci.*, **61**, 111 (2012).
8. G. Du, J. Li, W. K. Wang, C. Jiang, and S. Z. Song, *Corros. Sci.*, **53**, 2918 (2011).
9. J. Kovac, M. Leban, and A. Legat, *Electrochim. Acta*, **52**, 7607 (2007).
10. J. Kovac, C. Alaux, T. J. Marrow, E. Govekar, and A. Legat, *Corros. Sci.*, **52**, 2015 (2010).
11. D. H. Xia, S. Z. Song, J. H. Wang, J. B. Shi, H. C. Bi, and Z. M. Gao, *Electrochem. Commun.*, **15**, 88 (2012).
12. I. Szenes, G. Meszaros, and B. Lengyel, *Electrochim. Acta*, **52**, 4752 (2007).
13. D. Xia, S. Song, R. Zhu, Y. Behnamian, C. Shen, J. Wang, J. Luo, Y. Lu, and S. Klimas, *Electrochim. Acta*, **111**, 510 (2013).
14. D. H. Xia, C. Zhou, Y. H. Liu, J. H. Wang, C. W. Fu, K. Wang, and M. Li, *Electrochemistry*, **81**, 262 (2013).
15. T. Zhang, D. Y. Wang, Y. W. Shao, G. Z. Meng, and F. H. Wang, *Corros. Sci.*, **58**, 202 (2012).
16. M. R. Thakare, J. A. Wharton, R. J. K.Wood, and C. Menger, *Wear*, **267**, 1967 (2009).
17. J. Macak, P. Sajdl, P. Kucera, R. Novotny, and J. Vosta, *Electrochim. Acta*, **51**, 3566 (2006).
18. N. Zaveri, R. T. Sun, N. Zufelt, A. H. Zhou, and Y. Q. Chen, *Electrochim. Acta*, **52**, 5795 (2007).
19. C. Zhou, J. H. Wang, S. Z. Song, D. H. Xia, K. Wang, C. Shen, B. Luo, and J. B. Shi, *J. Wuhan Univ. Technol.*, **28**, 367 (2013).
20. D. H. Xia, S. Z. Song, W. Q. Gong, Y. X. Jiang, Z. M. Gao, and J. H. Wang, *J. Food Eng.*, ***113***, 11 (2012).
21. D. H. Xia, J. B. Shi, W. Q. Gong, R. J. Zhou, Z. M. Gao, and J. H. Wang, *Electrochemistry*, **80**, 907 (2012).
22. X. Jiang, S. Nesic, F. Huet, B. Kinsella, B. Brown, and D. Young, *J. Electrochem. Soc.*, **159**, C283 (2012).
23. M. Shahidi, R. F. Moghaddam, M. R. Gholamhosseinzadeh, and S. M. A. Hosseini, *J. Electroanal. Chem.*, **693**, 114 (2013).
24. A. M. Lafront, F. Safizadeh, E. Ghali, and G. Houlachi, *Electrochim. Acta*, **55**, 2505 (2010).
25. F. H. Cao, Z. Zhang, J. X. Su, Y. Y. Shi, and J. Q. Zhang, *Electrochim. Acta*, **51**, 1359 (2006).
26. A. M. Homborg, E. P. M. van Westing, T. Tinga, X. Zhang, P. J. Oonincx, G. M. Ferrari, J. H. W. de Wit, and J. M. C. Mol, *Corros. Sci.*, **66**, 97 (2013).
27. G. P. Quick, D. A. Eden, and R. J. Jacko, *Proc. Corrosion 2001 Conf.*, p. 123, NACE International Press, Houston (2001).
28. V. Kain, Y. Watanabe, and M. Kobayashi, *Proc. Corrosion 2001 Conf., p. 118,* NACE International Press, Houston (2001).
29. J. Hickling, D. F. Taylor, and P. L. Andresen, *Mater. Corros.*, **49**, 651 (1998).
30. P. Kucera, J. Macak, P. Sajdl, and R. Novotny, *Mater. Corros.*, **59**, 719 (2008).
31. J. C. Uruchurtu and J. L. Dawson, *Corrosion*, **43**, 19 (1987).
32. A. Chang and S. Song, *J. Chin. Soc. Corr. Pro.*, **32**, 247 (2012).